Interfacial separation between elastic solids with randomly rough surfaces: comparison between theory and numerical techniques

A. Almqvist[a,b,*], C. Campañá[c], N. Prodanov[b,d], B.N.J. Persson[b]

[a]*Division of Machine Elements, Luleå University of Technology, 971 87 Luleå, Sweden*
[b]*IFF, FZ-Jülich, 52425, Jülich, Germany*
[c]*University of Ottawa, Department of Chemistry, Ottawa, K1N 6N5, Canada*
[d]*Sumy State University, 2 Rimskii-Korsakov Str., 40007 Sumy, Ukraine*

Abstract

We study the distribution of interfacial separations $P(u)$ at the contact region between two elastic solids with randomly rough surfaces. An analytical expression is derived for $P(u)$ using Persson's theory of contact mechanics, and is compared to numerical solutions obtained using (a) a half-space method based on the Boussinesq equation, (b) a Green's function molecular dynamics technique and (c) smart-block classical molecular dynamics. Overall, we find good agreement between all the different approaches.

Keywords: Contact mechanics, randomly rough surfaces, elastic solids, pressure distribution, interfacial separation

1. Introduction

Modeling the contact mechanics between elastic solids with surfaces that are rough on multiple length scales is a challenging task. To perform such a task several theoretical approaches have been developed over the years. At the core of all the approaches lie approximations that relate to describing the shape of the contacting surfaces. In a seminal paper, Greenwood and Williamson (Greenwood & Williamson, 1966) (GW) proposed that the contact problem between two elastic rough surfaces could be reduced to the problem of one infinitely-hard rough surface acting on a flat elastic counterface. Within their model, the rough topography was described by a large collection of hemispherical asperities of uniform radius (which individually satisfied the Hertzian approximation) with a height distribution that followed a Gaussian law. This initial approach was later extended by Greenwood and Tripp (Greenwood & Tripp, 1970) by considering the presence of roughness on the two contacting surfaces. Further contributions to the original GW methodology have been proposed by

---

E-mail address: andreas.almqvist@ltu.se; Tel.: +49 920 492407; Fax: +46 920 491399

Whitehouse and Archard (Whitehouse & Archard, 1970), Nayak (Nayak, 1971), Onions and Archard (Onions & Archard, 1973), Bush et al. (Bush et al., 1975, 1979) and Whitehouse and Phillips (Whitehouse & Phillips, 1978, 1982). All these models rely on the definition of "asperity". The asperity concept itself has proved quite controversial and depends on the resolution of the instrument used to measure the surface profile(Poon & Bhushan, 1995). Another drawback of GW-type approaches is that using only a few parameters to describe the surfaces generates a one-to-many mapping possibilities, i.e., the same set of parameters can be deduced for surfaces obtained by completely different machining processes.

In spite of the great increase in computing power in the past decade, analytical theories are still very much needed to understand the contact mechanics of solids with surfaces that display roughness on more than three decades in length-scales. Theoretical models to tackle such problems rely on approximations and idealizations in order to analytically solve the equations of elasticity. For example, such equations can be exactly solved for the contact problem of a parabolic tip acting on a flat surface under the assumptions of linearly elastic, frictionless materials (Hertz model). Similarly, an exact solution can be obtained for the contact between a sinusoidal elastic surface and a rigid plane (Westergaard model) (Westergaard, 1939). The GW model and its extensions are further examples of how to deal with surface roughness in contact mechanics, resulting in simple analytic formulas. These easy-to-handle formulas have proved to be of great importance, and are frequently employed in the design process of new technical applications. The Hertz and the Westergaard models provide accurate representation of the mechanics of single asperities. In addition, the GW model describes approximately the (low squeezing-pressure) contact between surfaces exhibiting roughness on a single or a narrow distribution of length scales. However, most real surfaces have roughness over many decades of length scales. Here, the long range elastic coupling between the asperity contact regions, which is neglected in the GW model, is now known to strongly influence contact mechanics (Persson, 2008; Campañá et al., 2008). If an asperity is pushed downwards at a certain location, the elastic deformation field extends a long distance away from the asperity influencing the contact involving other asperities further away (Persson et al., 2002). We note that the lateral coupling between contact regions is important for arbitrary small squeezing pressure or load. The reason for this is that surfaces with roughness on many length scales can be considered as consisting of large asperities populated by smaller asperities, with the smaller asperities being populated by even smaller asperities and so on. Thus, when two solids are squeezed together by a very small external force, the distance between the macro-asperity contact regions will be very large, and one may be tempted to neglect the elastic coupling between the macro-asperity contact regions. However, the separation between the micro-asperity contact regions within a macro-asperity region will in general be very small, and one cannot neglect the elastic coupling between such micro-asperity contact regions. This latter effect is neglected in the GW theory, significantly limiting its prediction capabilities when applied to most real sur-

faces. Additionally, in the GW model the asperity contact regions are assumed to be circular (or elliptical) while the actual contact regions (at high enough experimental resolution) show fractal-like boundary lines (Borri-Brunetto et al., 2001; Pei et al., 2005; Persson & Yang, 2008). Therefore, because of their complex geometries, one should try to avoid explicitly invoking the nature of the contact regions when searching for an analytical methodology to solve the contact problem of two elastic rough surfaces.

Recently, an analytical contact mechanics model that does not use the asperity concept and becomes exact in the limit of complete contact has been developed by Persson (Persson, 2001, 2006, 2007; Yang & Persson, 2008; Persson & Yang, 2008). The theory accounts for surface roughness on all relevant length scales and includes (in an approximate way) the long range elastic coupling between asperity contact regions. In this theory the information about the surface enters via the surface roughness power spectrum $C(\mathbf{q})$, which depends on all the surface roughness wavevectors $\mathbf{q}$ components. The theory can be used to calculate the interfacial stress distribution $P(\sigma, \zeta)$, from which one can obtain the area of real contact as a function of the squeezing pressure p and the magnification ζ. Furthermore, the theory predicts the average interfacial separation $\bar{u}$ for any applied external load.

Besides analytical approaches, numerical algorithms (deterministic) have also been developed to understand the contact mechanics of elastic solids with rough boundaries. As the speed and memory capacity of computers increase, numerical methods have become a viable alternative to analytical methods when modeling surfaces of three-dimensional (3D) solids having surface roughness extending over at most three decades in length-scales. Nevertheless, simplifying assumptions about the material and the topography are still needed to ensure reasonable computational time windows. Much is still to be done in order to reach the capacity to numerically simulate real surfaces that may have roughness from the nanometer scale up to the macroscopic size of the system which could be cm.

Numerous numerical works have been reported in the literature aiming to solve the contact mechanics of two linear elastic solids with rough surfaces. The majority of these are half-space models in which the elastic deformation is related to the stress field at the surfaces of the solids through integral equations where the domain of integration is the boundary of the half-space. This type of approach is commonly referred to as boundary element method (BEM). Twenty years ago Lubrecht and Ioannides (Lubrecht & Ioannides, 1991) suggested applying multilevel techniques to facilitate the numerical solution of the BEM. With the same objective in mind Ren and Lee (Ren & Lee, 1994) implemented a moving grid method to reduce storage of the influence matrix when the conventional matrix inversion approach is used to solve this type of problem. Björklund and Andersson (Andersson & S. Björklund, 1994) extended the conventional matrix inversion approach by incorporating friction induced deformations. Alternative techniques that aim to solve the elastic contact of rough surfaces are the Fast Fourier Transform (FFT)-based method introduced by Ju and Farris (Ju & Farris, 1996) and a follow-up extension, based on a varia-

tional principle (Kalker, 1977), proposed by Stanley and Kato (Stanley & Kato, 1997). The contact between solids with realistic surface topographies under relatively small loads usually leads to plastic deformations. Tian and Bhushan, (Tian & Bhushan, 1996) based their theoretical model is based on a variational principle for linear elastic perfectly plastic materials. In this way, not only the in-contact topography and the corresponding pressure distribution but also the unloaded plastically deformed topography can be obtained for the case when the loading is high enough to cause yield. This model was further developed in the paper by (Sahlin et al., 2010) and this is also the BEM employed in the present work, but here we restrict the analysis to linear elastic materials.

In earlier works, the prediction of Persson's contact mechanics theory for the interfacial stress distribution $P(\sigma)$ and the contact area have been compared to numerical results obtained using the finite element method (FEM) (Hyun et al., 2004), molecular dynamics (Yang & Persson, 2008) and Green's function molecular dynamics (GFMD) (Campañá & Müser, 2007). In this paper, we will show how the theory can be extended to also predict the distribution of interfacial separations $P(u)$. This quantity is of crucial importance for problems like leak-rate of seals (Persson & Yang, 2008; Lorenz & Persson, 2010a,b) or mixed lubrication (Persson, 2010; Scaraggi et al., 2011; Lorenz & Persson, 2010c). The analytical results will be compared to numerical solutions obtained using (a) a half-space method based on the Boussinesq equation (BEM), (b) a Green's function molecular dynamics technique and (c) smart-block molecular dynamics.

2. Contact mechanics theory of Persson

Consider the frictionless contact between two elastic solids with Young's elastic moduli E_0 and E_1 and Poisson ratios ν_0 and ν_1. Assume that the surfaces of the two solids have height profiles $h_0(\mathbf{x})$ and $h_1(\mathbf{x})$, respectively. The elastic contact mechanics for the solids can be mapped into that of a rigid substrate with height profile $h(\mathbf{x}) = h_0(\mathbf{x}) + h_1(\mathbf{x})$ and a second elastic solid with a flat surface and Young's modulus E and Poisson ratio ν chosen so that (Johnson, 1985)

$$\frac{1 - \nu^2}{E} = \frac{1 - \nu_0^2}{E_0} + \frac{1 - \nu_1^2}{E_1}. \tag{1}$$

The main physical variables that characterize the contact between the solids are the stress probability distribution $P(\sigma)$ and the distribution of interfacial separations $P(u)$. These functions are defined as follows:

$$P(\sigma) = \langle \delta[\sigma - \sigma(\mathbf{x})] \rangle, \qquad P(u) = \langle \delta[u - u(\mathbf{x})] \rangle$$

where $\delta(..)$ is the Dirac delta function, and $\sigma(\mathbf{x})$ and $u(\mathbf{x})$ are the stress and the interfacial separation at point $\mathbf{x} = (x, y)$, respectively. The $\langle .. \rangle$ brackets denote ensemble averaging. Note that both $P(\sigma)$ and $P(u)$ have a delta function at the origin with its weight determined by the area of real contact i.e. given by $(1 - A/A_0)\delta(\sigma)$ and $(A/A_0)\delta(u)$. Here A_0 is the nominal contact area and A

the area of real contact projected on the xy-plane. Normalization conditions require that

$$\int d\sigma P(\sigma) = 1, \qquad \int du P(u) = 1$$

while

$$\int_{0+}^{\infty} d\sigma P(\sigma) = \frac{A}{A_0}, \qquad \int_{0+}^{\infty} du P(u) = \frac{A_0 - A}{A_0}.$$

Thus from the interfacial distribution of stresses or separations one can immediately determine the area of real contact A. The average interfacial stress (which must be equal to the applied pressure) $\bar{\sigma}$, and the average interfacial separation $\bar{u}$, can be obtained as

$$\bar{\sigma} = \int d\sigma \ \sigma P(\sigma), \qquad \bar{u} = \int du \ u P(u).$$

The stress and interfacial separation distribution functions, $P(\sigma)$ and $P(u)$, are determined by the elastic energy U_{el} stored in the asperity contact regions (see below). The elastic energy U_{el} is written as (Persson, 2002, 2006, 2008)

$$U_{\mathrm{el}} = \frac{EA_0}{4(1 - \nu^2)} \int d^2q \ qC(q)W(q) \tag{2}$$

where the surface roughness power spectrum is defined by

$$C(q) = \frac{1}{(2\pi)^2} \int d^2x \ \langle h(\mathbf{x})h(\mathbf{0})\rangle \mathrm{e}^{-i\mathbf{q}\cdot\mathbf{x}}. \tag{3}$$

The height profile $h(\mathbf{x})$ of any rough surface can be measured routinely nowadays on all relevant length scales using optical and stylus experiments.

For complete contact $W(q) = 1$ rendering an exact result for the expression of the energy above. In Ref. (Persson, 2002) it was argued that $W(q) = P(q) = A(\zeta)/A_0$ is the relative contact area when the interface is studied at the magnification $\zeta = q/q_0$ (where q_0 is the small-wavevector cut-off, usually chosen as π/L, where $L = \sqrt{A_0}$ is the linear size of the surface). The qualitative explanation for such an argument is that the solids will mainly deform in the regions where they make contact, and most of the elastic energy will arise from the contact regions. Nevertheless, using $W(q) = P(q)$ assumes that the energy (per unit area) in the asperity contact regions is just the average elastic energy (per unit area) as if complete contact would occur. This does not take into account that the regions where no contact occurs are those regions where most of elastic energy (per unit area) would be stored if complete contact would occur. Hence, we expect smaller stored elastic energy (per unit area) in the asperity contact regions than obtained using $W(q) = P(q)$. In Ref. (Yang & Persson, 2008; Persson, 2008; Campañá et al., 2011) we found that using

$$W(q) = P(q)\left[\gamma + (1 - \gamma)P^2(q)\right] = P(q)S(p, q), \tag{4}$$

with $\gamma \approx 0.45$ gives good agreement between theory and numerical calculations. Note that for complete contact $P(q) = 1$ and hence $W(q) = 1$ which reduces to

the exact result for the elastic energy in such a limit. On the contrary, in the limit of small contact, $P(q) << 1$ which yields $W(q) \approx \gamma P(q)$. For $\gamma \approx 0.45$ this results in an elastic energy which is a factor of 0.45 smaller than the elastic energy (per unit area) stored in the contact region in the case of complete contact. Recently, in an independent study, Akarapu et al. (Akarapu et al., 2010) found a value of $\gamma = 0.48$ after analyzing a variety of rough surfaces in contact with roughness down to the atomic scale, variable Poisson ratio and Hurst exponents of $H = 0.5$ and 0.8.

The contact mechanics formalism developed by Persson (Persson, 2001, 2006, 2007; Yang & Persson, 2008) is based on studying the interface between two contacting solids at different magnifications ζ. When the system is studied at the magnification ζ it appears as if the contact area (projected on the xy-plane) equals $A(\zeta)$, but when the magnification increases, it is observed that the contact is incomplete, and the surfaces in the apparent contact area $A(\zeta)$ are in fact separated by the average distance $\bar{u}(\zeta)$, see Fig. 2. The (apparent) relative contact area $A(\zeta)/A_0$ at the magnification ζ is given by (Persson, 2001; Yang & Persson, 2008)

$$\frac{A(\zeta)}{A_0} = \frac{1}{(\pi G)^{1/2}} \int_0^{p_0} d\sigma \ e^{-\sigma^2/4G} = \mathrm{erf}\left(\frac{p_0}{2G^{1/2}}\right) \tag{5}$$

where $p_0 = F_N/A_0$ is the nominal squeezing pressure and

$$G(\zeta) = \frac{\pi}{4}\left(\frac{E}{1-\nu^2}\right)^2 \int_{q_0}^{\zeta q_0} dq q^3 C(q) S(p,q). \tag{6}$$

In most applications $A/A_0 << 1$ and in this case one may use $S \approx \gamma$. The distribution of interfacial stress is given by (for $\sigma > 0$):

$$P(\sigma) = \frac{1}{2(\pi G)^{1/2}}\left[\exp\left(-\frac{(\sigma-p_0)^2}{4G}\right) - \exp\left(-\frac{(\sigma+p_0)^2}{4G}\right)\right]. \tag{7}$$

Let us define $u_1(\zeta)$ to be the (average) height separating the surfaces which appear to come into contact when the magnification decreases from ζ to $\zeta - \Delta\zeta$, where $\Delta\zeta$ is a small (infinitesimal) change in the magnification. $u_1(\zeta)$ is a monotonically decreasing function of ζ, and can be calculated from the average interfacial separation $\bar{u}(\zeta)$ and $A(\zeta)$ using (see Ref. (Yang & Persson, 2008))

$$u_1(\zeta) = \bar{u}(\zeta) + \bar{u}'(\zeta)A(\zeta)/A'(\zeta), \tag{8}$$

where

$$\bar{u}(\zeta) = \sqrt{\pi} \int_{\zeta q_0}^{q_1} dq \ q^2 C(q) w(q) \int_{p(\zeta)}^{\infty} dp' \ \frac{1}{p'} S(p',q) e^{-[w(q,\zeta)p'/E^*]^2}, \tag{9}$$

$E^* = E/(1-\nu^2)$, $p(\zeta) = p_0 A_0/A(\zeta)$ and

$$w(q,\zeta) = \left(\pi \int_{\zeta q_0}^{q} dq' \ q'^3 C(q')\right)^{-1/2}.$$
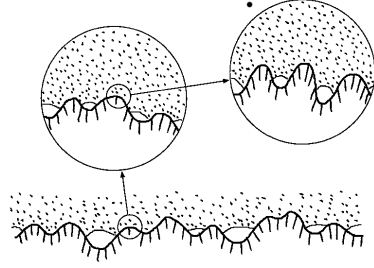
6

Figure 1: An elastic block (dotted area) in adhesive contact with a rigid rough substrate (dashed area). The substrate has roughness on many different length scales and the block makes partial contact with the substrate on all length scales. When a contact area is studied, at low magnification it appears as if complete contact occurs, but when the magnification is increased it is observed that in reality only partial contact has taken place.
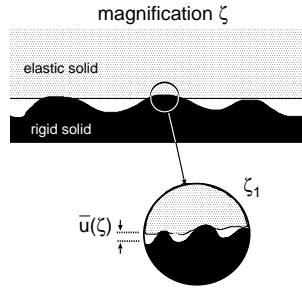

Figure 2: An asperity contact region observed at the magnification ζ. It appears that complete contact occurs in the asperity contact region, but when the magnification is increased to the highest (atomic scale) magnification ζ_1, it is observed that the solids are actually separated by the average distance $\bar{u}(\zeta)$.
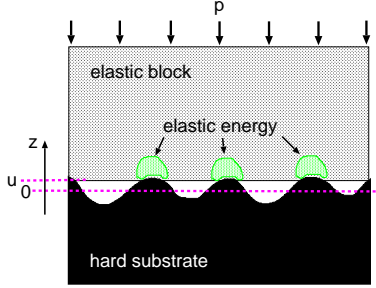
Figure 3: An elastic block squeezed against a rigid rough substrate. The separation between the average plane of the substrate and the average plane of the lower surface of the block is denoted by u. Elastic energy is stored in the block in the vicinity of the asperity contact regions.

The definition of the distribution of interfacial separations $P(u) = \langle \delta[u - u(\mathbf{x})] \rangle$ involves an ensemble average over many realizations of the surface roughness profile. If the surface roughness power spectra has a roll-off wavevector q_c which is much larger than $q_0 = \pi/L$, where L is the linear size of the surface, then performing an ensemble average is identical to averaging over the surface area. In this case we can write the distribution of interfacial separations as

$$P(u) = \frac{1}{A_0} \int_{A_0} d^2x \; \delta(u - u(\mathbf{x})). \tag{10}$$

The probability distribution is normalized

$$\int du \; P(u) = 1. \tag{11}$$

In the contact mechanics theory of Persson (Yang & Persson, 2008) the interface is studied at different magnification ζ. As the magnification increases, new short length scale roughness can be detected, and the area of (apparent) contact $A(\zeta)$ therefore decreases with increasing magnification. The (average) separation between the surfaces in the surface area which (appears) to move out of contact as the magnification increases from ζ to $\zeta + d\zeta$, is denoted by $u_1(\zeta)$ and is predicted by the Persson theory (see above). The contact mechanics theory of Persson does not directly predict $P(u)$ but rather the probability distribution of separation u_1 (see Ref. (Yang & Persson, 2008)):

$$P_1(u) = \frac{1}{A_0} \int_1^{\zeta_1} d\zeta [-A'(\zeta)] \; \delta(u - u_1(\zeta)). \tag{12}$$

Since $u_1(\zeta)$ is already an average, the distribution function $P_1(u)$ will be more narrow than $P(u)$, but the first moment of both distributions coincide and is equal to the average surface separation:

$$\bar{u} = \int_0^\infty du \; uP(u) = \int_0^\infty du \; uP_1(u).$$

To derive an approximate expression for $P(u)$ we write Eq. (10) as

$$P(u) = \frac{1}{A_0} \int_1^{\zeta_1} d\zeta [-A'(\zeta)] \langle \delta(u - u(\mathbf{x})) \rangle_\zeta. \tag{13}$$

Here $\langle .. \rangle_\zeta$ stands for averaging over the surface area which moves out of contact as the magnification increases from ζ to $\zeta + d\zeta$. Note that

$$\langle u(\mathbf{x}) \rangle_\zeta = u_1(\zeta). \tag{14}$$

A surface which moves out of contact as the magnification increases from ζ to $\zeta + d\zeta$ will have short-wavelength roughness with wavevectors larger than $q > \zeta q_0$. Thus the separation between these surface areas will not be exactly $u_1(\zeta)$, but will fluctuate around this value. One may take this into account by using

$$\langle (u(\mathbf{x}) - u_1(\zeta))^2 \rangle_\zeta \approx h_{\text{rms}}^2(\zeta), \tag{15}$$

where $h_{\text{rms}}^2(\zeta)$ is the mean of the square of the surface roughness amplitude including only roughness components with the wavevector $q > q_0\zeta$. We can write

$$h_{\text{rms}}^2(\zeta) = \int_{q>q_0\zeta} d^2q \ C(q), \tag{16}$$

where the surface roughness power spectra $C(q)$ can be calculated from the measured surface topography. Using the definition

$$\delta(u) = \frac{1}{2\pi} \int d\alpha \ e^{i\alpha u},$$

one can rewrite Eq. (13) as

$$P = \frac{1}{A_0} \int d\zeta \ [-A'(\zeta)] \frac{1}{2\pi} \int d\alpha \ \langle e^{i\alpha(u - u(\mathbf{x}))} \rangle_\zeta$$

$$= \frac{1}{A_0} \int d\zeta \ [-A'(\zeta)] \frac{1}{2\pi} \int d\alpha \ e^{i\alpha(u - u_1(\zeta))} \langle e^{i\alpha(u_1(\zeta)) - u(\mathbf{x}))} \rangle_\zeta.$$

To second order in the cummulant expansion

$$P \approx \frac{1}{A_0} \int d\zeta \ [-A'(\zeta)] \frac{1}{2\pi} \int d\alpha \ e^{i\alpha(u - u_1(\zeta)) - \alpha^2 \langle (u_1(\zeta) - u(\mathbf{x}))^2 \rangle_\zeta / 2},$$

or using Eq. (15):

$$P \approx \frac{1}{A_0} \int d\zeta \ [-A'(\zeta)] \frac{1}{(2\pi h_{\text{rms}}^2(\zeta))^{1/2}} \exp\left(-\frac{(u - u_1(\zeta))^2}{2h_{\text{rms}}^2(\zeta)} \right).$$

The above expression does not satisfy the normalization condition Eq. (11). We will therefore use instead

$$P \approx \frac{1}{A_0} \int d\zeta \ [-A'(\zeta)] \frac{1}{(2\pi h_{\text{rms}}^2(\zeta))^{1/2}}$$

$$\times \left[\exp\left(-\frac{(u - u_1(\zeta))^2}{2h_{\text{rms}}^2(\zeta)} \right) + \exp\left(-\frac{(u + u_1(\zeta))^2}{2h_{\text{rms}}^2(\zeta)} \right) \right]. \tag{17}$$

9

The added term in this expression can be considered as resulting from the cummulant expansion of

$$\frac{1}{A_0} \int_{A_0} d^2x \; \delta(u + u(\mathbf{x})).$$

Note that such a term vanishes for $u > 0$.

The theory described above predicts that for small squeezing pressures p the area of real contact is proportional to the squeezing pressure, while the interfacial separation depends logarithmically on p. Both results are related to the fact that when increasing p existing contact areas grow and new contact areas are formed in such a way that, in the thermodynamic limit (infinitely-large system), the interfacial stress distribution, and also the size distribution of contact spots, are independent of the squeezing pressure as long as these distributions are normalized to the real contact area A (Persson et al., 2005). In Ref. (Lorenz & Persson, 2009) (see also (Lorenz et al., 2010)) experimental results were presented to test the dependence of $\bar{u}$ on p. In the study a rubber block was squeezed against an asphalt road surface, and good agreement was found between the theory and experiments. The fact that $A \sim p$ for small load is also well tested experimentally, and is usually considered as the explanation for Coulomb's friction law which states that the friction force is proportional to the load or normal force.
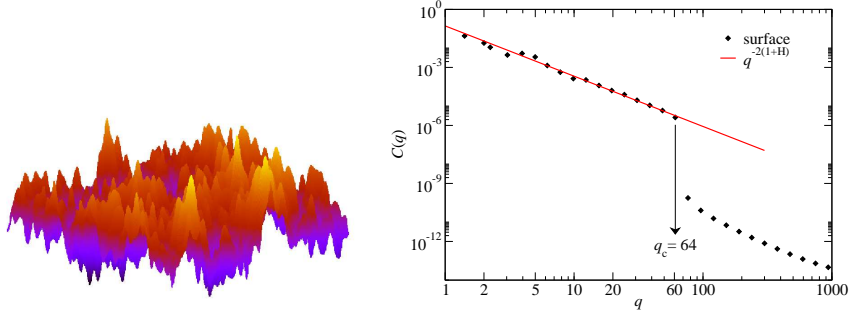

Figure 4: Graphical representation of a rough topography with Hurst exponent $H = 0.3$ and its corresponding height-height correlation function $C(q) = \langle |h(\mathbf{q})|^2 \rangle$ in Fourier space. The surface topography was created using a Fourier filtering technique and a hard cutoff $q_c = 64$ was imposed to it in Fourier space (in units of $2\pi/L$, where L is the linear size of the simulation cell). The continuous line represents the ideal algebraic scaling expected for the height-height correlation function of such a surface.

3. Numerical methods

When two elastic solids with rough surfaces come into contact, the elastic deformations perpendicular to the contacting plane extend into the solids a

characteristic length λ that could be as large as the contacting plane's lateral size L. Thus, in order to properly capture the mechanical response of the solids within the contact region, the elastic properties of the material have to be considered up to a distance L in the normal direction to the contacting plane. This is why standard algorithms that use a full representation of the system display a computational effort that scales with the system's size L^3. Such a scaling rapidly becomes a limitation when the linear dimension of the solids increases. The previous arguments explain why coarse-grained numerical techniques are needed when studying the contact mechanics of solids with more than two decades in surface roughness length-scales.

The theory developed in Sec. 2 for the distribution of interfacial separations $P(u)$ will be compared to the predictions of the following three different coarse-grained numerical methods: (a) a half-space method based on the Boussinesq equation (BEM), (b) a Green's function molecular dynamics technique (GFMD) and (c) smart-block classical molecular dynamics (MD). For this, we have considered the contact between an elastic block with a flat bottom surface and a randomly rough rigid substrate. Self affine fractal topographies with Hurst exponent values of $H = 0.3$, 0.5 and 0.8 (corresponding to the fractal dimension $D_{\mathrm{f}} = 3 - H = 2.7$, 2.5 and 2.2) are used to model the rigid substrate. Fig. 4 shows the surface topography $h(\mathbf{x})$ and the power spectrum $C(\mathbf{q})$ (on a log-log scale) of one of our surfaces with $H = 0.3$, hard cutoff $q_c = 64$ (in units of $2\pi/L$, where L is the linear size of the simulation cell) and rms-slope ~ 0.03.

Randomly rough substrate profiles were generated on a two-dimensional square grid with 2048×2048 mesh points. The surface heights were obtained via a Fourier Filtering Algorithm. In the case of the GFMD and BEM methods the elastic interactions within the original elastic block are chosen such that both Lame coefficients satisfy $\lambda = \mu = 1$. This choice of the coefficients results in a Young modulus of $E = 5/2$, a bulk modulus of $K = 5/3$, and a Poisson ratio of $\nu = 1/4$.

In the smart-block molecular dynamics simulations we used a smaller system size than in the other two numerical schemes. The surfaces were obtained by choosing every 4'th grid point from the original surfaces with 2048×2048 resolution. This procedure yielded surfaces with $N_x \times N_y = 512 \times 512$ mesh points. Since the original surfaces were quite smooth at short length scales (see the power spectrum in Fig. 4) the surfaces used in the smart-block MD simulations are expected to give the same contact mechanics as the original topographies. This was confirmed by comparing the MD results obtained for the 512×512 system sizes to those of the BEM method for the equivalent 2048×2048 systems. In our MD simulations the atoms in the bottom layer of the block are located on a simple square lattice with lattice constant $a = 2.6$ Å. The lateral dimensions of the block and substrate are $L_x = L_y = N_x a = 1331.2$ Å. The Young modulus of the block is $E = 250$ GPa and its Poisson ratio $\nu = 1/4$ identical to that of the other two schemes. Since no natural length scale exists in elastic continuum mechanics, one can directly compare the results of the smart-block MD model to those of the methods (a) and (b) by simply using a distance scaling factor of $(512/2048)a = 0.65$ Å, and a pressure (or stress) scaling factor of

$250/2.5 = 100$ GPa.

Next, we will provide a short technical review of the three numerical methods that we have employed in this work.

3.1. Boundary Element Method

Any contact mechanics problem can be solved by using a technique that minimizes the total potential energy of the system. Assuming frictionless linear elastic contact, the variational problem including constraints to be solved can be expressed as Eq. (18) (see, e.g., (Kalker, 1977), (Tian & Bhushan, 1996) and (Sahlin et al., 2010)):

$$\min_{p \geq 0} \left(\frac{1}{2} \int_A d^2x \, p(\mathbf{x}) u_z(\mathbf{x}) - \int_A d^2x \, p(\mathbf{x}) u_z^*(\mathbf{x}) \right), \tag{18}$$

where $p(\mathbf{x})$ is the pressure distribution, $u_z(\mathbf{x})$ is the associated elastic deformation and $u_z^*(\mathbf{x})$ is the prescribed surface displacements, equivalent to the roughness height coordinate (h) plus a constant controlling the prescribed shift. The first term describes the internal complementary energy due to elastic deflection, and the second term governs the contribution from the prescribed displacement $u_z^*(\mathbf{x})$. Note that $u(\mathbf{x}) = u_z(\mathbf{x}) - u_z^*(\mathbf{x})$. The Boussinesq relation between pressure and elastic deformation employed for this work may be formulated as

$$u_z(\mathbf{x}) = \frac{1 - \nu^2}{\pi E} \int d^2x' \frac{p(\mathbf{x}')}{|\mathbf{x} - \mathbf{x}'|}, \tag{19}$$

For the BEM method employed here, the complete system of equations consists of Eq. (18) and Eq. (19), and the force balance relation

$$\int_A d^2x \, p(\mathbf{x}) = F_N, \quad p(\mathbf{x}) \geq 0, \tag{20}$$

where F_N is the normal force or the applied load.

Numerically, the solution is achieved by employing the method outlined by (Sahlin et al., 2010), where the FFT algorithm is utilized to accelerate the computation of the elastic deflection. For the numerical results presented in this work, convergence of the solution process is reached when the following two convergence criteria are met:

- The force balance criterion that controls that the load generated by the contact pressure supports the applied load.

$$\frac{1}{F_N} \left| F_N - \int_A d^2x \, p(\mathbf{x}) \right| < 10^{-3},$$

- A geometric criterion that controls that points 'in-contact' lie sufficiently close to the contact plane.

$$\frac{\max_{\mathbf{x} \in A} |u_z(\mathbf{x}) - u_z^*(\mathbf{x})|}{\max_{\mathbf{x} \in A_0} h(\mathbf{x}) - \min_{\mathbf{x} \in A_0} h(\mathbf{x})} < 10^{-5}.$$

12

3.2. Greens Function Molecular Dynamics

Greens Function Molecular Dynamics (GFMD) (Campañá & Müser, 2006) is among the many simulation techniques available to find the equilibrium configuration of a mechanical system under the action of external loads. To achieve its goal GFMD solves the system's equations of motion for a set of initial/boundary conditions.

The potential energy of a linear elastic (harmonic approximation) solid is given by

$$V = \frac{1}{2} \sum_{ij} \sum_{\alpha\beta} k_{ij}^{\alpha\beta} u_{i\alpha} u_{j\beta} = \frac{1}{2} \sum_{ij} \mathbf{u}_i \cdot K_{ij} \cdot \mathbf{u}_j \tag{21}$$

where $\mathbf{u}_i = \sum_\alpha u_{i\alpha} \mathbf{e}_\alpha$ (where $\mathbf{e}_1 = \hat{x}$, $\mathbf{e}_2 = \hat{y}$ and $\mathbf{e}_3 = \hat{z}$ are orthogonal unit base vectors) is the deformation field at locations $\mathbf{x}_i$, and $K_{ij} = \sum_{\alpha\beta} k_{ij}^{\alpha\beta} \mathbf{e}_\alpha \mathbf{e}_\beta$ the force constant matrix. In thermal equilibrium, the $\mathbf{u}_i$ displacements will comply with the Boltzmann statistics with second moments given by

$$\begin{aligned}
\langle \mathbf{u}_i \mathbf{u}_j \rangle &= \frac{1}{Z} \int d\mathbf{u}_1 \cdots d\mathbf{u}_N \, \mathbf{u}_i \, \mathbf{u}_j \, e^{-\beta V} \\
&= k_B T \left[K^{-1} \right]_{ij},
\end{aligned} \tag{22}$$

with Z being the partition function. The equation above shows that one can obtain the force constant matrix $[K^{-1}]_{ij}$ from measuring the fluctuations in the second moments $\langle \mathbf{u}_i \mathbf{u}_j \rangle$. Furthermore, if the bottom surface of the solid is exposed to an external force field $\mathbf{F}_{\text{ext}}(\{\mathbf{u}\})$, all the degrees of freedom $\mathbf{u}_i$ that do not belong to the bottom surface can be integrated out (eliminated) yielding an equivalent problem for the bottom surface

$$V = \sum_{ij}^{surface} \frac{1}{2} \mathbf{u}_i \cdot \tilde{K}_{ij} \cdot \mathbf{u}_j - \sum_i^{surface} \mathbf{F}_{\text{ext}}^{(i)} \cdot \mathbf{u}_i \tag{23}$$

where $\tilde{K}_{ij}$ are new renormalized force constants. Renormalization takes place such that the new 2D surface obtained will deform under the action of the external field in exactly the same way as the bottom surface of our original 3D-solid. The matrix

$$[G]_{ij} = \left[\tilde{K}^{-1} \right]_{ij} = \frac{\langle \mathbf{u}_i \mathbf{u}_j \rangle}{k_B T}$$

is known as the Greens' function of the system. From Eq. (23) one obtains the equilibrium condition

$$\sum_j \tilde{K}_{ij} \cdot \mathbf{u}_j = \mathbf{F}_{\text{ext}}^{(i)}. \tag{24}$$

If the system is periodic in the (x, y)-plane (translational symmetry) one can use the Fourier transform to obtain decoupling of the modes in the $\mathbf{q} = (q_x, q_y)$-space as

$$\tilde{\mathbf{u}}(\mathbf{q}) = \tilde{G}(\mathbf{q}) \tilde{\mathbf{F}}_{\text{ext}}(\mathbf{q}). \tag{25}$$

13

Eq. (25) eliminates the non-local nature of the real-space solution of Eq. (24) while rendering an easily parallelizable scheme that can be used to simulate the contact mechanics of large systems. For a given interaction kernel $\tilde{G}(\mathbf{q})$, it is the implementation of Eq. (25) in a molecular dynamics fashion that lies at the core of GFMD.

Our GFMD implementation followed the approach described in previous works (Campañá & Müser, 2007; Campañá et al., 2008) where all the roughness is placed on the rigid substrate and the elasticity on a flat GFMD block. The interactions between the block and the rough substrate are modeled via a hard-wall potential. If the z-coordinate of an atom within the elastic block at location $\mathbf{x} = (x, y)$ crosses through $h(\mathbf{x})$, the corresponding interaction energy increases from zero to infinity. To obtain the value of the surface height $h(\mathbf{x})$ inside any square element of the grid, we employed interpolation via bi-cubic splines with zero partial and cross-derivatives at the corner grid points of each element.

Defining which block's atoms are in contact after equilibrium has been reached is done by analyzing the pressure distribution. In a fully equilibrated simulation, a wide pressure gap of several orders of magnitude would exist between the atoms that belong to the contact region and those which do not. This approach to defining the contacting status of a certain atom differs from geometrical ones where contact is defined by comparing the relative distance between the block's atom and the corresponding surface height at the local atomic position, as it is done within the BEM method.

3.3. Smart-block Molecular Dynamics

The smart-block molecular dynamics (MD) system is composed of an elastic block interacting with a rigid randomly rough substrate. The substrate and the bottom layer of the block consist of an array of 512×512 atoms. Periodic boundary conditions are applied in the xy-plane. The atoms in the bottom layer of the block form a simple square lattice with lattice constant $a = 2.6$ Å. The mass of a block atom is 197 amu, and its elastic parameters have already been mentioned at the beginning of this section.

In order to allow for a correct description of the long-wavelength components in the deformation field of the block, its thickness is chosen to be 1350.7 Å, which is slightly larger than its lateral dimension. The technical details of the smart-block implementation has been discussed elsewhere, see (Yang et al., 2006). The current smart-block consists of 12 atomic layers, and merging factors of 2 (in all 3 directions) are used for all layers, except the 1'st, 6'th and the 11'th. The smart-block contains 615780 atoms, and the total number of atoms involved in the simulations is 877924.

The atoms at the block-substrate interface interact via a repulsive potential $U(r) = 4\varepsilon (r_0/r)^{12}$, where r is the interatomic distance and the parameter ε corresponds to the binding energy between two atoms at the separation $r = 2^{1/6} r_0$. In our calculations we have used the values $r_0 = 3.28$ Å and $\varepsilon = 18.6$ meV. Zero temperature is maintained during the simulations using a Langevin thermo-stat (Griebel et al., 2007) and the equations of motion have been integrated

using Verlet's method (Griebel et al., 2007; Rapaport, 2004) with a time step of $\Delta t = 1$ fs.

In the present study the squeezing process proceeds as follows. The upper surface of the smart-block is moved towards the substrate at a constant velocity of $v = 5$ m/s with the block being compressed as its bottom layer approaches the substrate. The duration of simulations depends on the type of substrate and they last until a small enough separation between the bottom block layer and the substrate is achieved. Note that the thickness of the smart-block may influence the results. In particular, a too thin smart-block leads to noisy data with considerable deviation from the results of the other methods. Increasing the thickness of the smart-block beyond the lateral size of the surface ensures convergence in the results. One must add that the time dependencies of p and u are not monotonic, and some oscillations are observed, which may be attributed to elastic waves propagating in the block during its compression. Lowering the velocity of movement down to 2.5 m/s leads to a decrease in the amplitude of these oscillations. Moreover, the large u region in the dependence of pressure on u gets closer to the BEM results when a lower value of v is employed. This suggests that smaller values of v should be used in future studies.

4. Results and discussion

We first consider the dependency $p(\bar{u})$ of the pressure p on the average interfacial separation $\bar{u}$. Figure 5 shows $p(\bar{u})$ obtained using the analytical theory (black lines), the BEM (blue symbols), GFMD (green symbols) and the smart-block MD approach (red lines). The figure includes results for surfaces with Hurst exponents of $H = 0.3$, 0.5 and 0.8. Note that the analytical theory has been developed for infinite systems, which will have infinitely high asperities, therefore always leading to a certain degree of contact between the solids. The small systems sizes utilized in the numerical simulations resulted in the highest asperities exceeding by only a factor of three (above the average plane) the root-mean-square roughness of the surfaces. This explains the sharp drop in the pressure in the computer simulation curves at the height threshold value established by the tallest asperity.

In the smart-block MD simulations, the finite range of the interaction potential between the block atoms and the surface atoms resulted in a non-unique way of defining $\bar{u}$. In the current work, to obtain $\bar{u}$ a small contribution δu of about 4 Å has been subtracted from the difference $z_1 - z_0$ in the average position of the interfacial atoms of the block and the substrate. How to find the best δu is a rather difficult question, and several alternative ways exist to accomplish such a goal. Here we have used that in the continuum limit the $P(u)$ distribution must display a maximum (delta-like behaviour) at its origin. In smart-block simulations the maximum in $P(u)$ gets shifted to a non-zero surface separation due to the finite range of the interaction potential. This behavior is shown in Fig. 6 for two different external pressure values. Thus, shifting the MD probability distribution $P(u)$ towards the origin by δu is necessary in order to be able to compare with the GFMD and BEM continuum mechanics results.
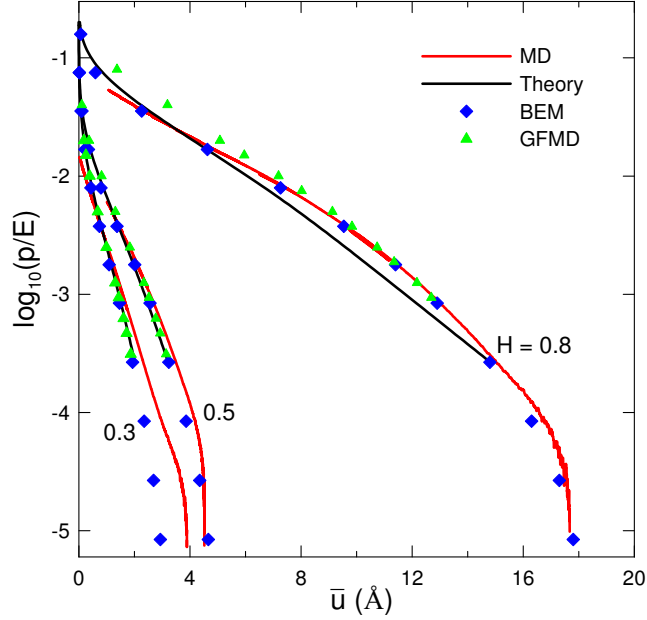
15

Figure 5: The relation between the applied squeezing pressure p and the average interfacial separation $\bar{u}$.

Persson's contact mechanics theory predicts that the average interfacial separation in the large $\bar{u}$ range is related to the applied pressure p via $p \sim \exp(-\bar{u}/u_0)$, where u_0 is of order of the root-mean-square roughness of the undeformed rough surface. This result, already confirmed by experimental works (Lorenz & Persson, 2009; Lorenz et al., 2010), differs drastically from the prediction of GW-like asperity models which instead yield a dependency of the type $p \sim \exp(-b\bar{u}^2)$ with b being a constant. The origin for those differences, an exponential decay predicted by Persson's theory and a Gaussian decay obtained by GW, is the omission of the long-range elastic deformations within asperity contact models which also results in very different morphologies for the contact regions as illustrated in Figs. 7 and 8.

Figure 7 shows the contact morphology generated for a $H = 0.8$ rough surface at three different external pressures, $p = 0.0032E$, $0.008E$, $0.012E$, when the long-range elastic deformations are taken into account. In Figure 8 we show the morphologies obtained (for identical values of the "true" contact area A) when a bearing area model is utilized. The lack of long-range elastic coupling in the latter model produces qualitatively different contact morphologies (compare Figures 7 and 8). Thus, when elastic deformations are considered, the contact regions become less compacted, with fractal-like boundaries, and are distributed over a larger fraction of the nominal contact area than those predicted by the asperity model in Fig. 8.
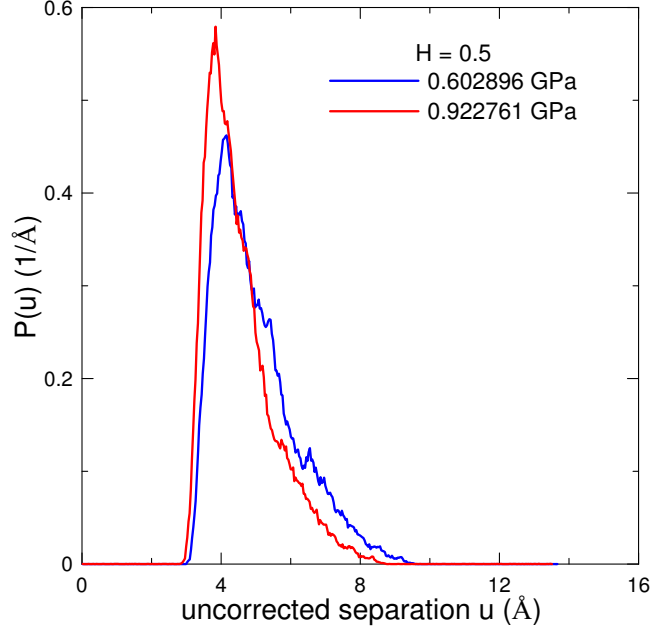
16

Figure 6: Distribution of interfacial separations for the substrate with $H = 0.5$ obtained in classical MD simulations.

A first comparison between the probability distribution $P(u)$ of interfacial separations u obtained using the BEM, smart-block MD and GFMD methodologies at the squeezing pressures $p = 0.79, 0.78$ and 0.75 GPa, respectively, is displayed in Figure 9. As shown, slight changes in applied pressure did not vary significantly the general shape of $P(u)$. This is indicative of the individual consistency in the implementation of each numerical technique. Further comparison of the numerical methods to the theoretical predictions is included in Fig. 10 in the limit of (a) non-contact, (b) low-pressure region and (c) medium-to-high pressure region. The red lines correspond to the predictions of Persson's contact mechanics theory (Eq. (17)) while the blue lines have been obtained from GFMD (in (b)) and BEM ((a) and (c)). All the numerical results correspond to a single realization of the rough surface which explains the rather large fluctuations (noise) in the $P(u)$ data. In particular, the ensemble averaged $P(u)$ for the non-contact case (zero squeezing pressure, $p = 0$) must follow a Gaussian law as given by the theory curve. However, the lack of a small wavevector roll-off (or cutoff) in the surface roughness power spectra implied that numerous independent topographies would have to be considered in order to achieve averages that closely represent the thermodynamic limit. Due to the large computational effort involved in such a task no further attempt to improve our statistics was performed.

As already mentioned in the methods section, the original contact mechanics

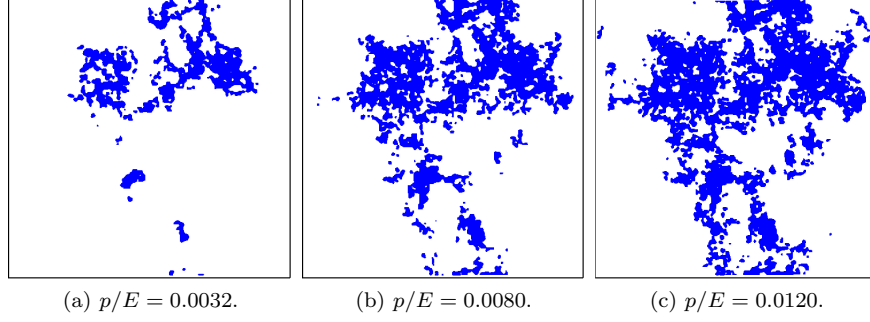(a) $p/E = 0.0032$.   (b) $p/E = 0.0080$.   (c) $p/E = 0.0120$.

Figure 7: Contact morphologies for the $H = 0.8$ surface at three different contact pressures; (a) $p = 0.0032E$, (b) $p = 0.0080E$ and (c) $p = 0.0120E$ when long-range elastic deformations are considered. The fractional contact areas are $A/A_0 = 0.066$, 0.161 and 0.238, respectively
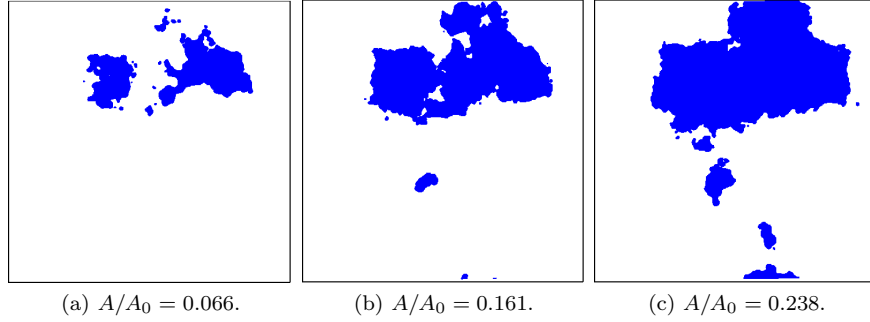

(a) $A/A_0 = 0.066$.   (b) $A/A_0 = 0.161$.   (c) $A/A_0 = 0.238$.

Figure 8: Contact morphologies predicted by a bearing area model for the same "true" contact area A values as in Figure 7 but where long-range elastic coupling has been neglected.

18
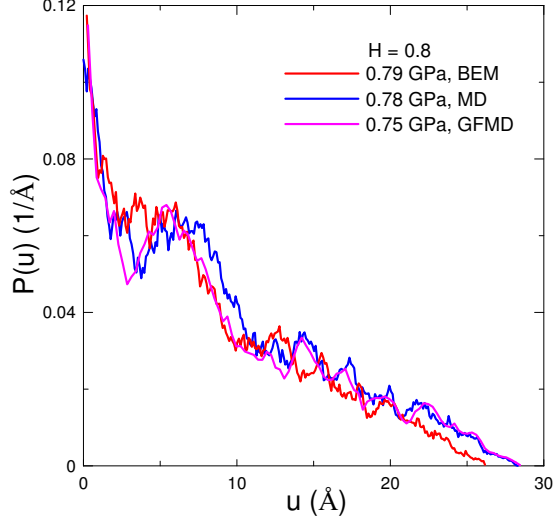
Figure 9: Probability distribution $P(u)$ of interfacial separations u, obtained using the BEM, MD and GFMD methods for $p = 0.79$, 0.78 and 0.75 GPa, respectively.

theory of Persson does not directly predict $P(u)$ but instead $P_1(u)$ (distribution of boundary-line averaged interfacial separations) which is a much sharper function than the interfacial separation distribution. The individual behaviour of both functions for the $H = 0.8$ surface at a squeezing pressure of $p = 0.003E$ is plotted in Fig. 11. In the figure the analytical $P(u)$ predicted using Eq. (17) (red curve) and $P_1(u)$ (green line) (Eq. (12)) are compared to the numerically exact distribution generated from GFMD simulations (blue curve). Because the bin size of the $P(u)$ and $P_1(u)$ computations was smaller than that of the numerical GFMD study the delta function at the origin $u = 0$ barely shows in the first two cases. Nevertheless, based on the results presented in Figs. 9, 10 and 11 we feel confident to conclude that the extension presented in this work to compute $P(u)$ within the framework of Persson's original contact theory yields quite reasonable quantitative predictions when compared to numerically exact simulations of the same contact problem.

Another physical variable of interest in contact mechanics studies is the ratio A/A_0 between the real area of contact and the nominal contact area. With the help of Persson's theory one can derive expressions that relate A/A_0 to the average interfacial separation $\bar{u}$. Next, the predictions from such a relation can be compared to those of numerical calculations. Figure 12 depicts the fractional contact ratio obtained in theoretical and numerical simulations of rough surfaces with variable Hurst exponents over a wide pressure region. As depicted, in the low-pressure regime (large $\bar{u}$ zone) all approaches converged to the same limit. This is further proof of the suitability of the numerical techniques discussed
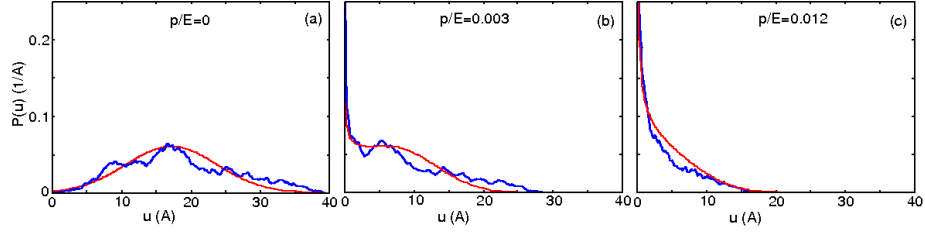
19

Figure 10: Probability distribution $P(u)$ for several squeezing pressure values. The red line corresponds to the theoretical predictions and the blue to numerical simulations (in (a) and (c) using BEM and in (b) using GFMD).
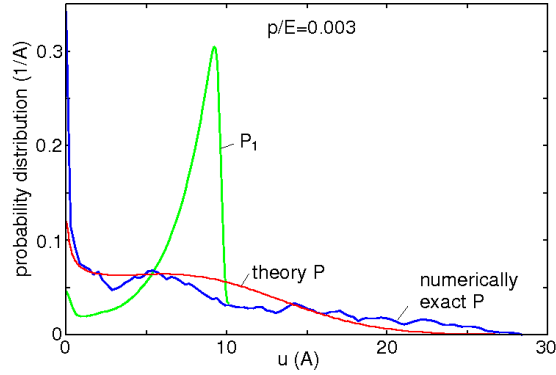

Figure 11: Probability distribution $P(u)$ for the squeezing pressure $p = 0.003E$ obtained in a numerically exact calculation (blue curve), and by applying the theoretical result from (Eq. (16)) (red curve). Also shown is the theory prediction (Eq. (17)) for the distribution $P_1(u)$ of boundary-line averaged interfacial separations (green curve).

20

here to study the contact mechanics of elastic solids with randomly-rough surfaces under engineering conditions. As the pressure and H exponent increase, discrepancies arised between GFMD and the other approaches. In future works the cause for such discrepancies in the high pressure region must be further investigated.
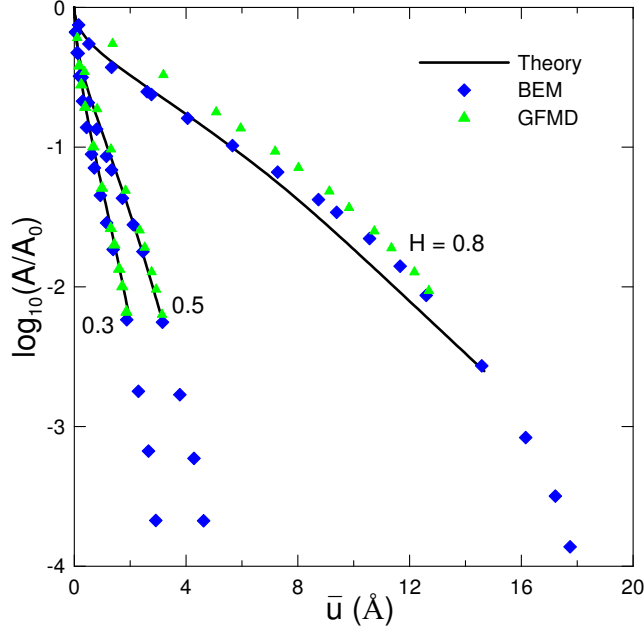

Figure 12: The contact area A/A_0 as a function of average interfacial separation $\bar{u}$ for the $H = 0.3$, 0.5 and 0.8 surfaces.

5. Summary and conclusions

The contact mechanics theory developed by Persson has been extended to allow for the calculation of the distribution of interfacial separations $P(u)$. The theory has been applied to study the contact mechanics of a flat elastic solid squeezed against an infinitely-hard randomly rough substrate. Three different coarse-grained numerical approaches have been used to simulate the same problem: (a) the boundary element method (BEM), (b) Green's function molecular dynamics (GFMD) and (c) smart-block molecular dynamics. The theoretical predictions have been compared to those of the numerical methods.

All the numerical methods and the analytical theory gives very similar results for the pressure p and the fractional contact area A/A_0, as a function of the average interfacial separation $\bar{u}$. In agreement with some earlier numerical studies when find a linear proportionality between real area of contact A and the

applied load at low loads, and a logarithmic relation between the average interfacial separation and the applied pressure in the same load regime (Akarapu et al., 2010; Campañá et al., 2011; Lorenz & Persson, 2009; Lorenz et al., 2010). We note that these functional forms are those predicted by Persson's theory thus pointing to the capabilities of the theory to properly account for long-range elastic deformations.

The distribution of interfacial separations $P(u)$ was studied in the low-to-medium pressure regions and our results showed that the theory gives quantitative predictions of reasonable accuracy for $P(u)$ when compared to the results obtained from numerically-exact calculations. However, the rather small system sizes used in the numerical calculations resulted in finite size effects (noise) for large interfacial separations. Among the numerical schemes we note that the BEM model, based on a FFT-accelerated implementation of the Boussinesq equation, is fast and accurate over the whole range of squeezing pressures. The GFMD method is also computationally very fast, but its results deviated from the expected solution for large values of the roughness exponent and high pressures. While the cause for such discrepancies needs to be investigated, we note that it lies within the current numerical implementation of the GFMD code and not in the GFMD theory which is in principle exact. Lastly, the smart-block classical MD is the most computationally demanding approach. Nevertheless, in contrast to BEM and GFMD, it naturally includes adhesion and friction in an atomistic way, and its current implementation can be applied within the full pressure range.

References

Akarapu, S., Sharp, T., Robbins, M.O., 2010. Stiffness of contacts between rough surfaces. arXiv:10.1479v1.

Andersson, S., Björklund, S., 1994. A numerical method for real elastic contacts subjected to normal and tangential loading. Wear 179, 117–122.

Borri-Brunetto, M., Chiaia, B., Ciavarella, M., 2001. Incipient sliding of rough surfaces in contact: a multiscale numerical analysis. Comput. Methods Appl. Mech. Eng. 190, 6053–6073.

Bush, A.W., Gibson, R.D., Thomas, T.R., 1975. The elastic contact of a rough surface. Wear 35, 87–111.

Bush, A.W., Gibson, R.D., Keogh, G.P., 1979. Strongly anisotropic rough surfaces. Transactions of the ASME. Journal of Lubrication Technology 101, 15–20.

Campañá, C., Müser, M. H., 2006. Practical Green's function approach to the simulation of elastic semi-infinite solids. Phys. Rev. B 74, 075420.

Campañá, C., Müser, M. H., 2007. Contact mechanics of real vs. randomly rough surfaces: A Green's function molecular dynamics study. Europhys. Lett. 77, 38005.

Campañá, C., Müser, M.H., Robbins, M.O., 2008. Elastic contact between self-affine surfaces: comparison of numerical stress and contact correlation functions with analytic predictions. J. Phys.: Condens. Matter 20, 354013.

Campañá, C., Persson, B.N.J., Müser, M.H., 2011. Transverse and normal interfacial stiffness of solids with randomly rough surfaces. J. Phys.: Condens. Matter 23, 085001.

Greenwood, J.A., Williamson, J.B.P., 1966. Contact of nominally flat surfaces. Proc. R. Soc. Lond. A 295, 300–319.

Greenwood, J.A., Tripp, J.H., 1970. The contact of two nominally flat rough surfaces. Proc. IME 185, 625–633.

Griebel, M., Knapek, S., Zumbusch, G., 2007. Numerical Simulation in Molecular Dynamics. Springer, Berlin, Heidelberg.

Hyun, S., Pei, L., Molinarie, J.F., Robbins, M.O., 2004. Finite-element analysis of contact between elastic self-affine surfaces. Phys. Rev. E 70, 026117.

Johnson, K.L., 1985. Contact Mechanics. Cambridge University Press, Cambridge.

Ju, Y., Farris, T.N., 1996. Spectral analysis of two-dimensional contact problems. Trans. ASME. J. Tribol. 118, 320–328.

Kalker, J.J., 1977. Variational principles of contact elastostatics. IMA J. Appl. Math. 20, 199–219.

Lorenz, B., Persson, B.N.J., 2009. Interfacial separation between elastic solids with randomly rough surfaces: comparison of experiment with theory. J. Phys.: Condens. Matter 21, 015003.

Lorenz, B., Carbone, G., Schulze, C., 2010. Average separation between a rough surface and a rubber block: Comparison between theories and experiments. Wear 268, 984–990.

Lorenz, B., Persson, B.N.J., 2010a. Leak rate of seals: Effective-medium theory and comparison with experiment. Eur. Phys. J. E 31, 159–167.

Lorenz, B., Persson, B.N.J., 2010b. Europhys. Lett. 90, 38002.

Lorenz, B., Persson, B.N.J., 2010c. Time-dependent fluid squeeze-out between solids with rough surfaces. Eur. Phys. J. E 32, 281–290.

Lubrecht, A.A., Ioannides, E., 1991. A fast solution of the dry contact problem and the associated sub-surface stress field, using multilevel techniques. Trans. ASME. J. Tribol. 113, 128–133.

Nayak, R.P., 1971. Random process model of rough surfaces. Lubr. Technol. Trans. ASME 93, 398–407.

Onions, R.A., Archard, J.F., 1973. The contact of surfaces having a random structure. J. Phys. D 6, 289–304.

Pei, L., Hyun, S., Molinari, J.F., Robbins, M.O., 2005. Finite element modeling of elasto-plastic contact between rough surfaces. J. Mech. Phys. Solids 53, 2385–2409.

Persson, B.N.J., 2001. Theory of rubber friction and contact mechanics. J. Chem. Phys. 115, 3840;

Persson, B.N.J., Bucher, F., Chiaia, B., 2002. Elastic contact between randomly rough surfaces: Comparison of theory with numerical results. Phys. Rev. B 65, 184106.

Persson, B.N.J., 2002. Adhesion between an elastic body and a randomly rough hard surface. Eur. Phys. J. E 8, 385–402.

Persson, B.N.J., Albohr, O., Tartaglino, U., Volokitin, A.I., Tosatti, E., 2005. On the nature of surface roughness with application to contact mechanics, sealing, rubber friction and adhesion. J. Phys. Condens. Matter 17, R1.

Persson, B.N.J., 2006. Contact mechanics for randomly rough surfaces. Surf. Sci. Rep. 61, 201.

Persson, B.N.J., 2007. Relation between interfacial separation and load: A general theory of contact mechanics. Phys. Rev. Lett. 99, 125502.

Persson, B.N.J., 2008. On the elastic energy and stress correlation in the contact between elastic solids with randomly rough surfaces. J. Phys.: Condens. Matter 20, 312001.

Persson, B.N.J., Yang, C., 2008. Theory of the leak-rate of seals. J. Phys.: Condens. Matter 20, 315011.

Persson, B.N.J., 2010. Fluid dynamics at the interface between contacting elastic solids with randomly rough surfaces. J. Phys.: Condens. Matter 22, 265004.

Poon, C.Y., Bhushan, B., 1995. Comparison of surface roughness measurements by stylus profiler, AFM and non-contact optical profiler. Wear 190, 76–88.

Rapaport, D.C., 2004. The Art of Molecular Dynamics Simulation, second ed. Cambridge University Press, Cambridge.

Ren, N., Lee, Si C., 1994. Effects of surface roughness and topography on the contact behavior of elastic bodies. Trans. ASME. J. Tribol. 116, 804–811.

Sahlin, F., Larsson, R., Marklund, P., Lugt, P.M., Almqvist, A., 2010. A mixed lubrication model incorporating measured surface topography. Part 1: theory of flow factors. Proc. IME J J. Eng. Tribol. 224, 335–351.

Saito, Y., 2004. Elastic lattice Green's function in three dimensions. J. Phys. Soc. Jap. 73, 1816.

Scaraggi, M., Carbone, G., Persson, B.N.J., Dini, D., 2011. Submitted to Soft Matter.

Stanley, H. M., Kato, T., 1997. FFT-based method for rough surface contact. Trans. ASME. J. Tribol. 119, 481–485.

Tian, X., Bhushan, B., 1996. A numerical three-dimensional model for the contact of rough surfaces by variational principle. J. Tribol. 118, 33–42.

Westergaard, H.M., 1939. Bearing pressure and cracks. ASME J. Appl. Mech. 6, 49–53.

Whitehouse, D.J., Archard, J.F., 1970. The properties of random surface of significance in their contact. Proc. R. Soc. Lond. A 316, 97–121.

Whitehouse, D.J., Phillips, M.J., 1978. Discrete properties of random surfaces. Phil. Trans. R. Soc. Lond. A 290, 267–298.

Whitehouse, D.J., Phillips, M.J., 1982. Two-dimensional discrete properties of random surfaces. Phil. Trans. R. Soc. Lond. A 305, 441–468.

Yang, C., Tartaglino, U., Persson, B. N. J., 2006. A multiscale molecular dynamics approach to contact mechanics. Eur. Phys. J. E 19, 47–58.

Yang, C., Persson, B. N. J., 2008. Contact mechanics: contact area and interfacial separation from small contact to full contact. J. Phys.: Condens. Matter 20, 215214.